The Effect of Valve Lift on In-Cylinder Flow, Performance and Emissions in a Turbocharged DI Diesel Engine

S. E. Razavi
Associate Professor - University of Tabriz
Razavi@Tabrizu.ac.ir

M. Rabiei*
Msc Student - University of Tabriz
Mahdi.Rabiei@Gmail.com

Faculty of Mechanical Engineering, University of Tabriz

Correiponding Authors
Received: Dec. 1, 2009
Accepted in Revised From: Feb. 16, 2010

Abstract

A computational optimization was performed for a direct-injection diesel engine using three-dimensional modeling. Fully transient CFD analyses of different valve profile strategies for the intake and compression strokes were performed to evaluate the effects on both engine performance and in-cylinder flow-field evolution. The turbulence model was used along with the second order linear upwind scheme. Modifications were applied to intake valve for five different valve lift profiles. Organized flow structures (i.e., swirl) and turbulent flow patterns were investigated in order to address the rules for ad-hoc strategies aiming at finding the best trade-off between the engine performance and pollutant emission. At first, results for the base case were validated against experiments at maximum power operation (2000 rpm); subsequently, four valve lift profiles, were performed. Relative valve profiles were proved to influence the flow field within the combustion chamber, and, therefore, the subsequent spray evolution and fuel combustion which confirmed the importance of an ad-hoc optimization.

Keywords: *Swirl. Valve Lift. CFD. NOx. Soot*

Introduction

Due to restrict legislation of emission level and environmental concerns for engine-out , soot and UHC, there is a need to develop engines which have only not superior fuel economy but also lower emissions. In diesel engine, in-cylinder flow is known as one of the main parameters influencing the engine performance. Because of the conservation of angular momentum, the intake flow velocity produces rotation around the cylinder axis (swirl) or normal to cylinder axis (tumble). Both of these structures store the kinetic energy during the intake and compression strokes and that energy is converted into turbulence near the top dead center. Thus, higher levels of turbulence and high swirl values are very important for a good mixture and fast combustion [1]. By intakes simulations, one can describe all events occur in the combustion chamber during intake, compression and expansion.

CFD optimization of diesel engine performance and emission using variable intake valve has been developed by Shrivastava et al [1]. This technique optimizes the engine operating variables by KIVA3v-Generic Algorithm optimization, which performs a full engine cycle simulation within the framework of a GA code. A 1-D gas dynamics code for the simulation of the gas exchange, coupled with the KIVA3v models the spray, combustion and emissions formation. The effect of swirl and tumble ratios on emissions reduction was found to be the most prominent at high speed, and low load. At high speed the swirl is effective in enhancing the rate of mixing, and, thus, lower emissions.

Cantore et.al [2] utilized the STAR-CD to optimize the in-cylinder flow patterns in high speed DI diesel engine. They investigated the effect of the adaption of different valve cam profiles to the intake valves, on the in-cylinder flow evolution. The modification of the valve profile affects the in-cylinder flow structure and swirl intensity, and has a strong influence on both engine performance and pollutants.

Hear, analyses are performed using the AVL_FIRE_CFD licensed by University of Tabriz. In the present study, the effect of different valve lifting profiles on the emissions and flow pattern are investigated. It is hoped that engine manufactures will have the ability to reach engine performance goals and meet emissions regulations in less time and at a lower cost.

Governing equations

A 3-D simulation was carried out using the SIMPLE algorithm [3]. For continuity and turbulence equations, second order upwind scheme and for momentum and energy equations, the SMART scheme [4] were used. The turbulent flow within the combustion chamber was modeled using a modified RNG k-ε turbulence model [5]. The wave breakup model of Reitz [6] was used for spray dynamics, atomization and breakup of fuel. In this model, fuel drop parcels are injected with a characteristic size equal to the nozzle hole diameter. For the spray-wall impingement, the model of Naber and Reitz was applied [7]. Diesel combustion modeling is splitted into two regimes, namely ignition and combustion. The ignition model used is the Shell model, consisting of 8 generic reactions and 5 generic species. The following expressions describe the species and reactions [8]:

Initiation: $$F + Ox \overset{\omega_i}{\rightarrow} 2\bar{R} \quad (1)$$

Propagation: $$\bar{R} \overset{\omega_p}{\rightarrow} \bar{R} + P \quad (2)$$

$$\bar{R} \overset{\omega_1}{\rightarrow} \bar{R} + B \quad (3)$$

$$\bar{R} \overset{\omega_4}{\rightarrow} \bar{R} + Q \quad (4)$$

$$\bar{R} + Q \overset{\omega_p}{\rightarrow} \bar{R} + B \quad (5)$$

Branching: $$B \overset{\omega_b}{\rightarrow} 2\bar{R} \quad (6)$$

Linear Termination: $$\bar{R} \overset{\omega_3}{\rightarrow} I \quad (7)$$

Quadratic Termination: $$2\bar{R} \overset{\omega_t}{\rightarrow} I \quad (8)$$

Where F is the hydrocarbon fuel (C_nH_{2m}), $\overline{R}$ is the total radical pool, B is the Branching agent, Q is an intermediate species, P is the oxidize product and I inactive species. The reaction rate of the kinetic scheme of Halstead [8] was applied. A significant part of combustion was thought to be mixing-controlled. Hence, interactions between the turbulence and chemical reactions had to be considered. The model described in this section combines a laminar and a turbulent time scale to an overall reaction rate. The time rate of change of a species m due to this time scale can be written as follows [9]:

$$\frac{dY_m}{dt} = -\frac{Y_m - Y_m^*}{\tau_c} \quad (9)$$

where Y_m is the mass fraction of the species m and Y_m* is the local instantaneous thermodynamic an equilibrium value of the mass fraction. The τ_c is the characteristic time for the achievement of such equilibrium. It is sufficient to consider the seven species including Fuel, O_2 , N_2 , CO_2 , CO , H_2, and H_2O to be able to predict the thermodynamic equilibrium temperature accurately enough. The characteristic time τ_c of a laminar and a turbulent time scale can be described by:

$$\tau_c = \tau_l + f.\tau_t \tag{10}$$

where *f* is the delay coefficient. The laminar time scale is derived from an Arrhenius type reaction rate:

$$\tau_l = A^{-1}\left[C_xH_y\right]^{0.75}[O_2]^{-1.5}exp\left(\frac{E_a}{RT}\right) \tag{11}$$

The turbulent time scale is proportional to the eddy break-up time:

$$\tau_t = C_2\frac{K}{\varepsilon} \tag{12}$$

where *k* and *ε* are the turbulent kinetic energy and dissipation rate, respectively which are obtained from the *k-ε* model. The delay coefficient *f* simulates the increasing influence of turbulence on combustion after ignition and can be calculated from the reaction progress *r*:

$$f = \frac{1 - e^{-r}}{0.632} \tag{13}$$

$$r = \frac{Y_{CO_2} + Y_{H_2O} + Y_{CO} + Y_{H_2}}{1 - Y_{N_2}} \tag{14}$$

This whole approach is conceptually consistent with the model of Magnussen[10]. The initiation of combustion relies on laminar chemistry. Turbulence starts to have an influence after combustion events have already been observed. The combustion will be dominated by turbulent mixing effects in regions of $\tau_l << \tau_t$. The laminar time scale is not negligible in regions near the injector where high velocities cause a very small turbulent time scale. Auto ignition is calculated by the Shell Model which is integrated in the specific model description. The formation of *NOx* is described by the extended Zeldovich mechanism [11]. The overall soot formation rate is modeled as the difference between soot formation and soot oxidation [12]:

$$\frac{dM_{soot}}{dt} = \frac{dM_{form}}{dt} - \frac{dM_{oxide}}{dt} \tag{15}$$

where the soot formation is [13]:

$$\frac{dM_{form}}{dt} = A_f M_{fv} P^{0.5} exp\left(-\frac{E_f}{RT}\right) \tag{16}$$

with A_f as the preexponential factor, M_{fv} is the fuel vapor mass, *P* is the pressure and E_f is the activation energy. The soot oxidation rate is adopted from Nagle and Strickland-Constable [14]:

$$\frac{dM_{oxide}}{dt} = \frac{6MW_c}{\rho_s D_s} M_s R_{tot} \tag{17}$$

where MW_c is the carbon molecular weight, P_s is the soot density, D_s is the average soot diameter, M_s is the soot mass and R_{tot} is the net reaction rate.

Engine specifications

The engine model used in this study is a product of PERKINS Company. The main engine specification and operating conditions for the base case are presented in Table 1.

Grid features

In operating condition the mesh should move in order to simulate the change of valve and piston positions with crank angle.

Table 1. Engine Specifications and operating conditions.

Number of Intake Valves	1 per cylinder
Bore × Stroke (mm)	100 × 127
Compression Ratio	17.5:1
Engine Speed (rpm)	2000
Intake Pressure (kPa)	128
Intake Temperature (k)	320
Start of Injection (deg btdc)	4
Duration of Injection (deg)	17
Number of Nozzle Orifice × Diameter (mm)	5 × 0.276
IVC to EVO (deg atdc)	-146 to 95
Displacement (lit)	3.99
Rate of Fuel Injected (kg/h)	15.22
Combustion Chamber	ω

At a specified crank angle, mesh rezoning maps the flow variable data from the first mesh to the second. The rezones are unacceptable distortions of cells caused either by the mesh movement or the use of different grid resolutions to speed up the simulation. In the present work, to simulate the valve and piston position accurately at any crank angle, 32 groups of meshes were created from IVO to EVO. Near

the opening and closing of intake valve, at each 10 degrees the rezoning was performed and for the other steps, at each 20 degrees it was repeated. The exhaust process, however, is not the concern of this paper so the exhaust valve and port were not included in computational mesh. It should be noted that the valve overlapping period is small (20 degrees). Furthermore, at IVO, the corresponding lift of the exhaust valve is about 0.5 mm. Under these conditions, the assumption of zero overlapping in the simulations is fully acceptable.

Figure 1 represents the configuration at TDC in a STL (stereo lithography) format file, which was used to depict the engine geometry in FIRE software. Figure 2 shows the computational grid with boundary zones shown on it. The computational domain includes the intake port and valve, the cylinder and the piston bowl. To avoid excess computation, after closing the intake valve, the intake port and valve were eliminated. To ensure grid independence, three calculations of the compression stroke, starting at IVC results (with no valve motion), were performed and compared to the base state for the pressure and emissions. For the first, second, and third calculations, the maximum cell sizes are 1.8, 1.9, 2.0 millimeters respectively which the results show no variation between two first cases. So in this paper, 1.8(mm) maximum cell size was selected.

The number of cells in the intake process varies from 179000 to 337000. In compression and expansion processes, the number of cells varies from 213000 at IVC, to 25000 at TDC. The predominant of cells are hexahedral, but because of the complexity of geometry, in particular regions, some tetrahedral or transition cells have also been used.

Various valve lift profiles

The intake process for five different intake valve lift profiles was simulated using the FIRE software. Figure 3 shows the five valve lift profiles, together with the piston position. These profiles are referred to as Base lift and Lift 2 to Lift 5. Lift 2 and Lift 3 have 20% increase and 20% decrease in maximum valve lift with respect to Base lift, respectively. Lift 4 and Lift 5 have 10% increase and 15% decrease in valve opening duration with respect to Base lift, respectively. All the five valve lift cases had the same initial conditions at the start of simulation (i.e., at IVO) that are reprsented in table 1.

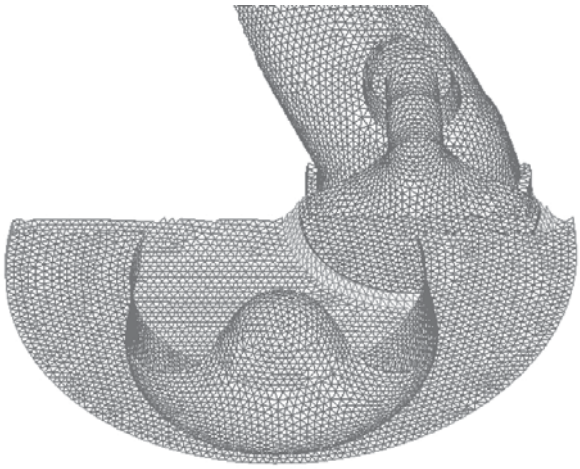

Fig 1. STL format of model.

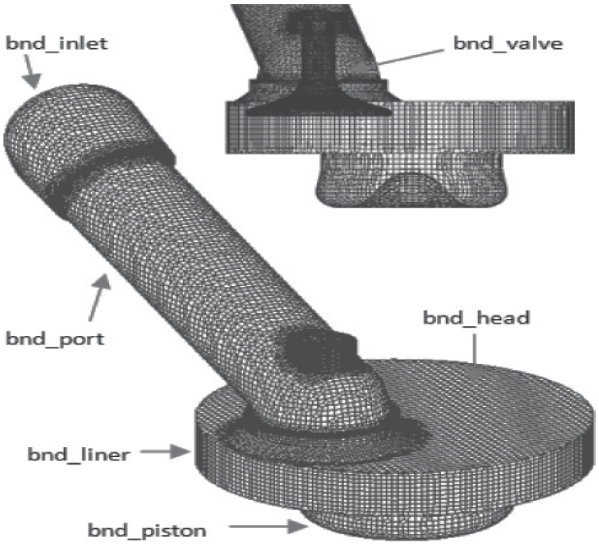

Fig 2. Computational grid with boundary zones.

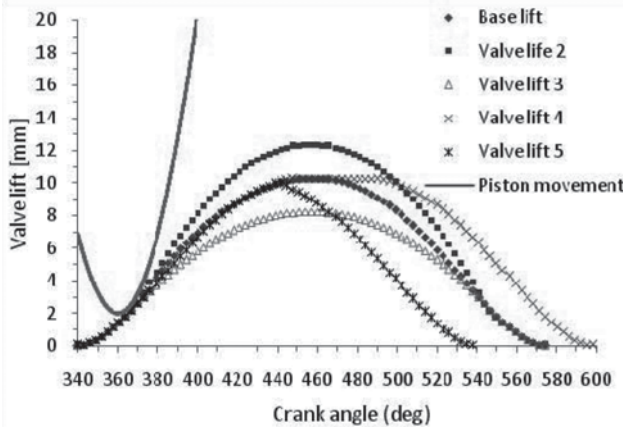

Fig 3. Different intake valve lift profiles and the piston position from the head.

Numerical results and validation

In this section, a comparison between experiments and simulation is presented in order to assess the accuracy of the subsequent predictions. At first, the full load maximum power engine speed (2000 rpm) is considered for the base state. The figure 4 presents the comparison in terms of in-cylinder pressure. As it is observed from the figure, a good agreement between the experimental and numerical results does exist. Also, Table 2 shows the comparison between the numerical and the experimental results at EVO.

Table 2. Comparison between numerical and experimental data for the base state.

Parameters	Experimental	Numerical	% error
NO¬x (g/kW-h)	7.81	8.22	5.2
Soot (g/kW-h)	0.27	0.29	5.6
bsfc(g/kW-h)	245.48	258.67	5.4
Brake Power(kW)	62.00	58.84	5.1

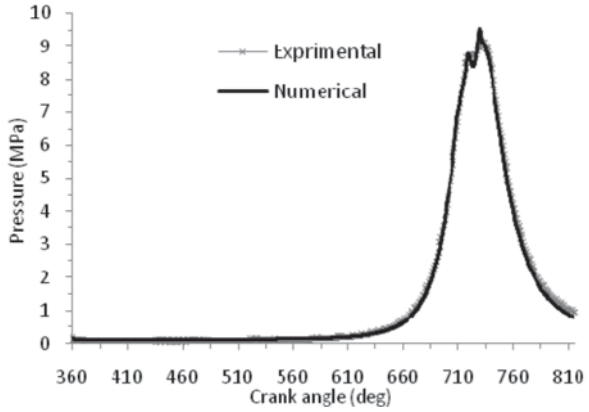

Fig 4. In-cylinder pressure comparison for the base state.

Flow field characterization

In this section, the results of the considered different valve lift profiles were compared with those of the Base state. The type and duration of intake valve lifting affects the in-cylinder trapped mass at IVC and volumetric efficiency. Figures 5 and 6 show the trapped mass and volumetric efficiency for different valve lifts. As it is clearly visible, the breathing capacity appears to be only slightly affected by the relative valve profile modification in Lift (2) and Lift (3) in comparison to the Base state. Because of the presence of the turbocharger, which is able to compensate the small variation in valve curtain flow interactions, the variations are small. For Lift (4) in which the time duration of opening is larger than that of the Base state, both the trapped mass and volumetric efficiencyare decreased. This could be due to the fact that during the compression stroke, air goes back into the intake manifold (as it was open during the compression stroke, too). Since Lift (5) had an early IVC as compared to base state and Lift (4), the in-cylinder trapped mass at IVC and volumetric efficiency are reduced due to the early valve closure which a ctually reduced the amount of the inlet mass. Figures 7 and 8 show the predicted swirl ratio variation during the intake, compression and expansion strokes. At the start of the induction stroke, the swirl ratio has fluctuations. It is appeared evidently that swirl ratio reaches its maximum intensity in the vicinity of the maximum valve lift. During the compression stroke, the swirl ratio decreases slightly. Indeed the vortices produced during the intake stroke cannot preserve their intensity during the compression stroke. At the late stages of the compression, the swirl levels tend to increase and have a local peak probably due to the flow entrance within the piston bowl. When the acceleration of the piston goes down, the swirl ratio increases and when the velocity of the piston goes down, it leads to the reduction of the swirl level. By comparison of the lift 2, lift 3, and Base state, it can be seen that the higher maximum lift with constant valve open duration leads to a higher swirl level. It can also be observed from lift 4, lift 5, and Base state that the longer valve open duration causes the higher swirl ratio.

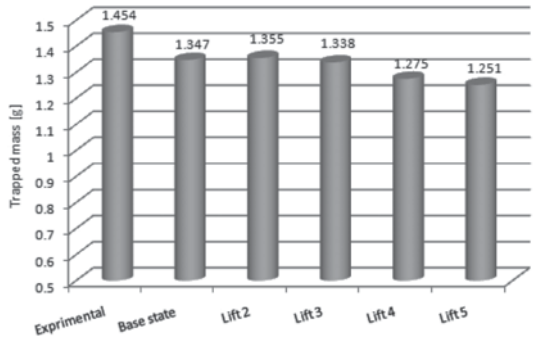

Fig 5. In-cylinder trapped mass of the different intake valve lift profiles for one cycle.

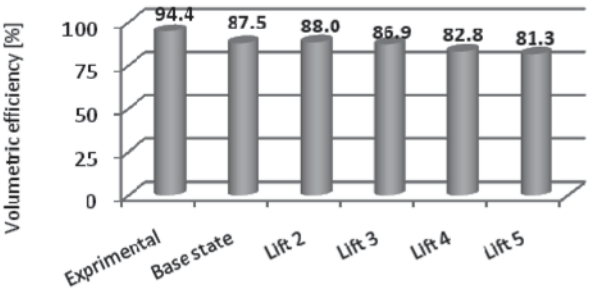

Fig 6. Volumetric efficiency of the different intake valve lift profiles for one cycle.

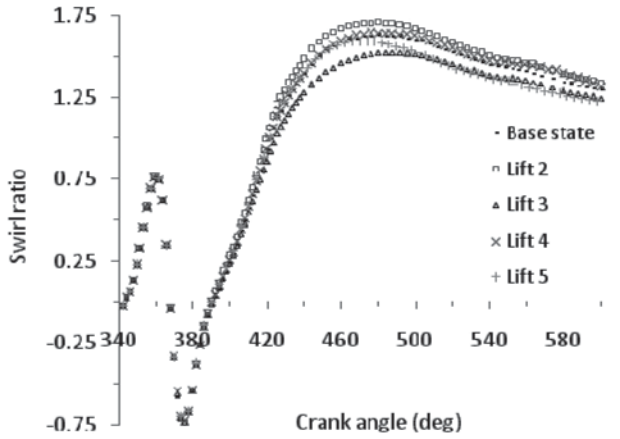

Fig 7. Variation of Swirl ratio vs. crank angle during the intake process for different valve lift profiles.

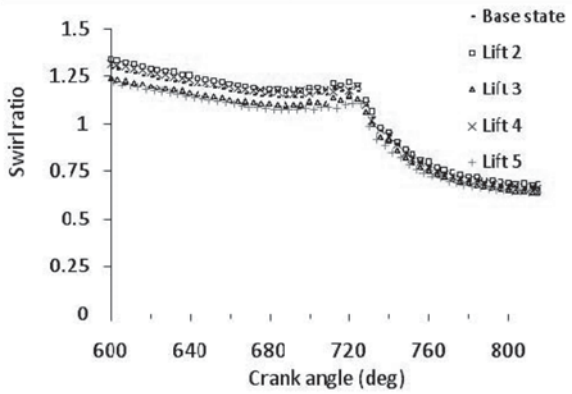

Fig 8. Variation of Swirl ratio vs. crank angle during the compression and expansion process for different valve lift profiles.

The streamlines and velocity vectors are shown in Figure 9 at maximum valve lift of Base state. The tumble motion can be seen below the intake valve and at the other zones, the swirl motion is obvious. Figure 10 compares the pressure between all cases. As it can be seen, because of the trapped mass in the first three cases, the pressure curves also are very close to each other. By lowering the volumetric efficiency, the pressure would also go down.

Fig 9. Streamlines and velocity vectors.

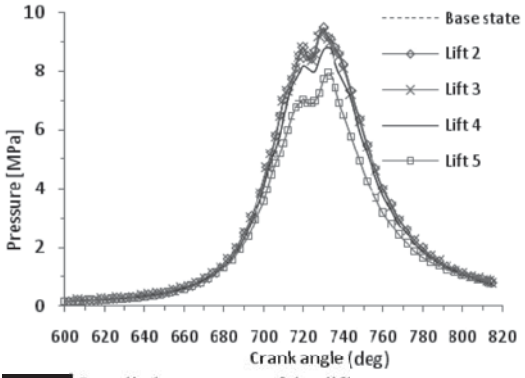

Fig 10. In-cylinder pressures of the different intake valve lift profiles.

Performance and pollutants

In this section, for all cases the performance and pollutants were studied during the expansion stroke. Figure 11 shows the heat release rate and injection rate. The small improvement in the flow field results in slight variations in the heat release rate. The enhancement of the flow motion leads to a slightly improved ignition and faster combustion. From the figure, four stages of the combustion can be observed. These are ignition delay, premixed combustion, diffusion combustion, and late combustion phases. Because of the small period of ignition delay and retard of injection, the small fraction of fuel was burnt in the premixed combustion phase.

Figure 12 shows the interaction of streamline flow and spray droplet at 5 ATDC in Base State. As it can be seen, the evolution in piston bowl and cylinder cause the distribution the of spray droplet from the center line of it. Further distribution of spray droplet leads to better fuel-air mixing and combustion.

Figure 13 represents the comparison of *NOx* mass fraction during the expansion stroke. As it can be seen, the

better flow structure, yields the higher *NOx*. The comparison of *NOx* at the end of expansion stroke was shown in Figure 14.

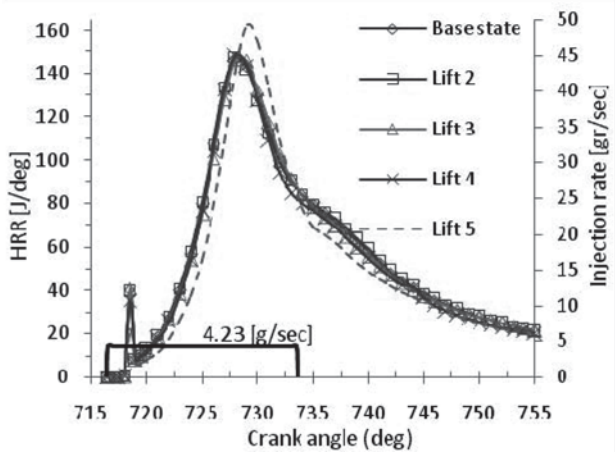

Fig 11. Heat release rates of the different intake valve lift profiles.

The soot mass fraction which was represented in Figures 15 and 16 show the soot emission at the end of the expansion stroke. Better in-cylinder flow-field leads to accessible air for oxidation of soot and lower soot emission. By increasing the swirl level, the soot concentration reduces, because of the faster mixing with air, decrease. Figure 17 shows the growth of *NOx* and soot versus the mean equivalence ratio for the Base state and represents the quality of the emission formation. The *NOx* increases near the stoichiometry equivalence ratio. The highest equivalence ratio causes the highest soot emission. In rich equivalence ratio, the formation of soot grows.

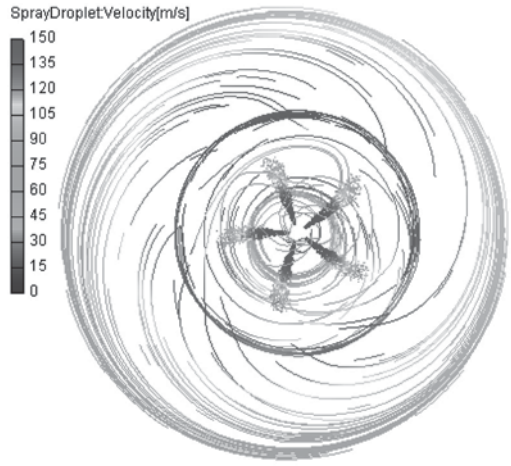

Fig 12. Interaction between streamlines flow and spray droplet at 5 ATDC for base state.

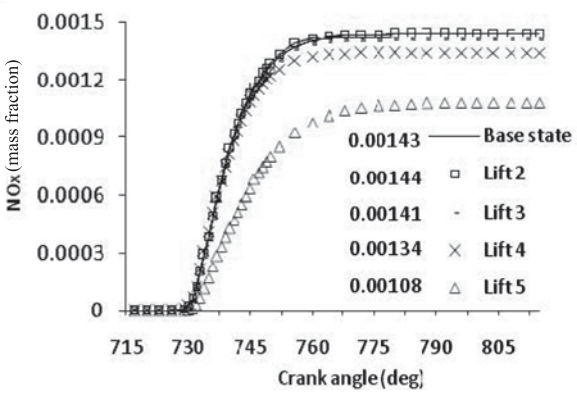

Fig 13. comparison of *NOx* mass fraction.

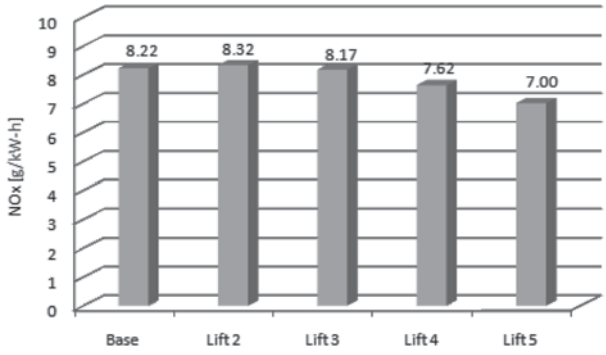

Fig 14. Comparison of *NOx* at EVO.

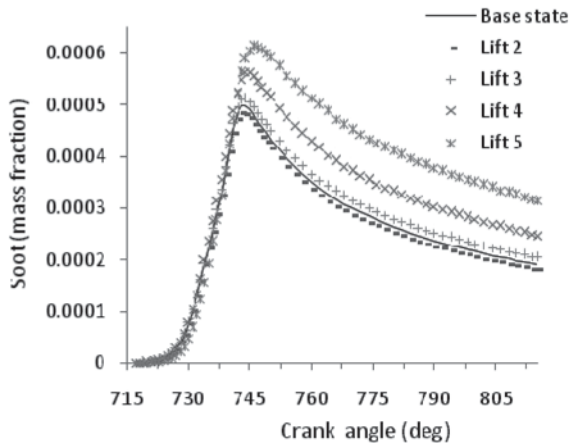

Fig 15. comparison of Soot mass fraction.

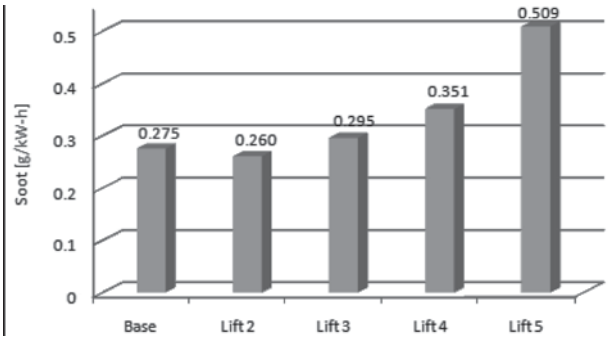

Fig 16. Comparison of Soot at EVO.

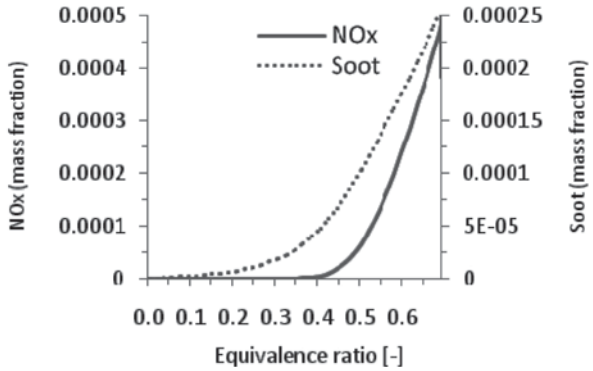

Fig 17. Growth of *NOx* and Soot vs. mean in-cylinder equivalence ratio for the base state.

In Figure 18 the quality relevance between O_2 , *NOx* and soot mass fraction, temperature and equivalence ratio at 20 ATDC for Base state, can be seen.

This figure shows when the local temperature is high and the local equivalence ratio is close to 1 (stoichiometry mixture), the *NOx* formation gets higher than the other zones. It can be observed that soot was formed in rich combustion zones where the oxygen diffusion to combustion zones was not adequate in order to reach the stoichiometric state.

Figures 19 and 20 show the brake power and *bsfc* for various valve lift profiles. It appears evidently that by increasing the volumetric efficiency, the brake power also increases and the *bsfc* comes down. The predicted optimum in Lift (2), has significantly improved fuel economy over the Base state.

As it was presented in the previous study, it can be seen that, by increasing the brake power and *NOx*, the *bsfc* and soot decrease. So the trade-off between these competitive parameters should be considered. In this study the optimum case is Lift (2) and because the increment of *NOx* versus the decrement of soot is ignorable.

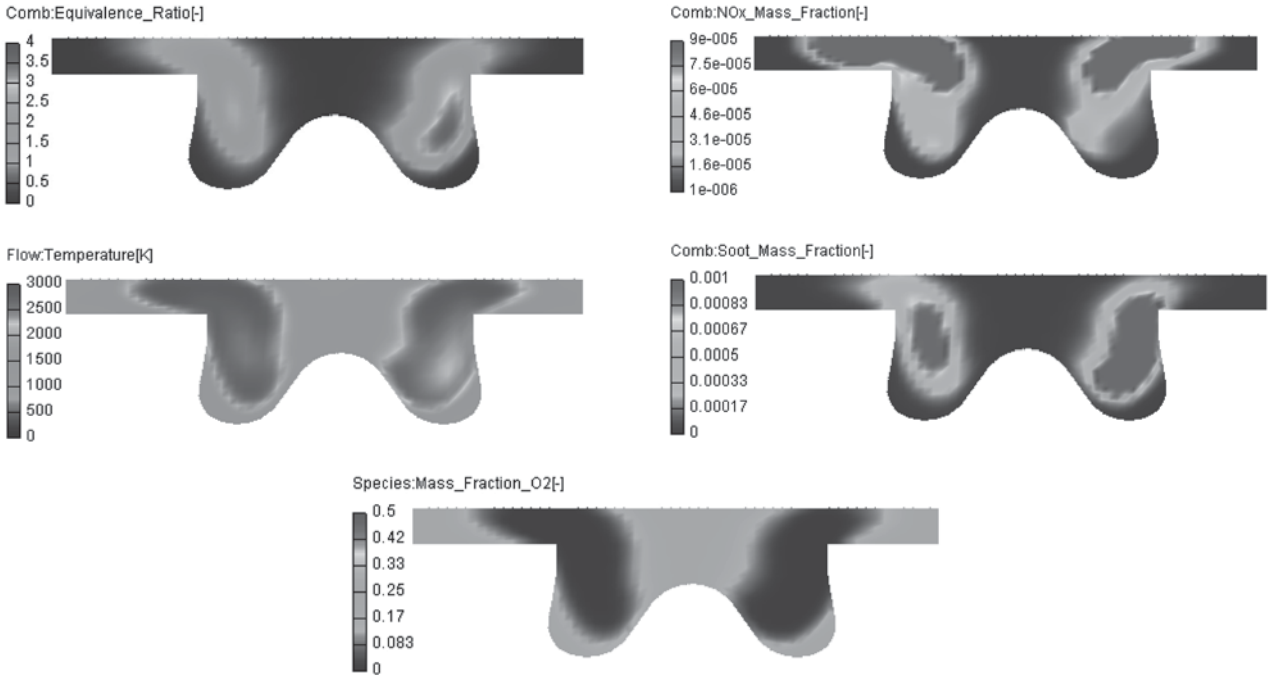

Fig 18. Qualitative demonstration of numerical results at 20 ATDC for base state.

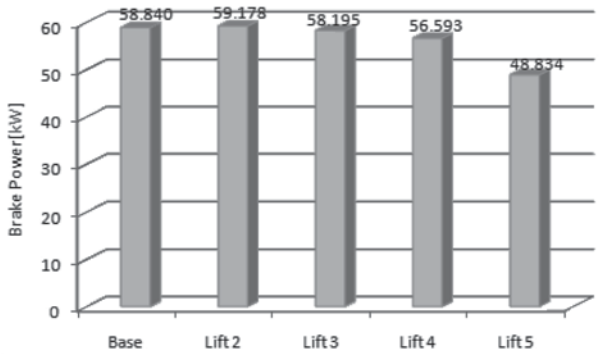

Fig 19. Comparison of brake power for different intake valve lifts.

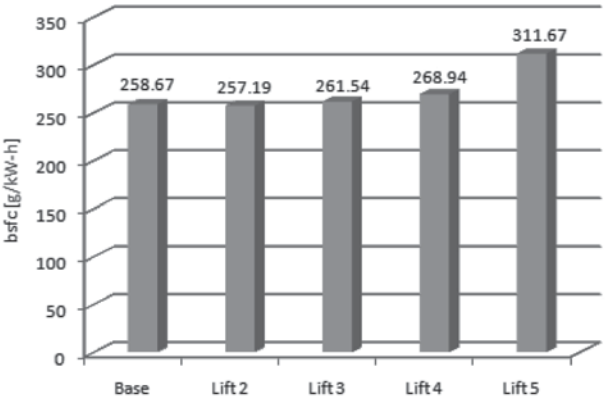

Fig 20. Comparison of bsfc for different intake valve lifts.

Conclusion

This paper investigates the effects of different intake valve profiles at power speed on in-cylinder flow, engine emission and performance by means of 3-D flow analysis for a DI diesel engine. By growing the maximum intake valve lift, with the same valve opening duration, the volumetric efficiency and trapped mass were slightly grown. Increase or decrease of intake valve opening duration was led to considerable reduction of volumetric efficiency versus Base state. By large increment of this parameter, the air reverse flow into the manifold and its reduction cause early IVC and lowering trapped mass. At the second half of the induction stroke, by raising the maximum valve lift, the swirl level was enhanced. By extending the valve opening duration, the swirl ratio was improved and vice versa. By increase and decrease of maximum valve lift up to 20%, there is no considerable effect on the pressure, due to the little change in volumetric efficiency. However, extension and contraction of valve opening duration reduces the pick pressure. By raising maximum valve lift up to 20%, little increase in *NOx* and brake power, and considerable decrease in soot and *bsfc* occurred. Unfortunately, because of reverse behaviors of pollutants and *bsfc*, the accomplishment of major technologies that lead to *NOx* reduction, an increase in soot and *bsfc*, and vice versa. So the trade-off between these parameters should be taken into account.

Acknowledgement

This work was supported by the Iranian Fuel Conservation Organization (IFCO). The authors would like to thank MOTORSAZAN manufacturer of diesel engine that provided the experimental data used for the code validation.

References

[1]. Shrivastava, R., Hessel, R., Reitz, R. D., "CFD Optimization of DI Diesel Engine Performance and Emissions Using Variable Intake Valve Actuation with Boost Pressure, EGR and Multiple Injections," SAE Paper NO. 2002-01-09559, 2002

[2]. Cantore, G., Fontanesi, S., Gagliardi, V., Malaguti, S., "CFD optimisation of the in-cylinder flow patterns in a small unit displacement HSDI Diesel Engine for off-highway applications," SAE Paper NO. 06SETC-161, 2006

[3]. Karki, K.C., Patankar, S.V. "Pressure-based calculation procedure for viscous flows at all speeds in arbitrary configurations," AIAA Journal, Vol. 27, pp. 1167-1174, 1989.

[4]. Gaskell, P.H., Lau, A.K.C. "Curvature Compensated Convective Transport: SMART, A New Boundedness Preserving Transport Algorithm." Int. J. for Numerical Methods in Fluids, Vol. 8, pp. 617-641, 1988.

[5]. Yakhot, V., Orszag, S.A., Thangam, S., Gatski, T.B., and Speziale, C.G.: 'Development of turbulence models for shear flows by a double expansion technique', Phys. Fluids, A4(7), pp. 1510–1520.

[6]. Reitz, R. D. "Modeling Atomization Processes in High-Pressure Vaporizing Sprays," Atomization and Spray Technology, 3, 309-337, 1987.

[7]. Naber, J.D. and Reitz, R.D. "Modeling Engine Spray/Wall Impingement" SAE- 880107.

[8]. Halstead, M., Kirsch, L., Quinin, C., "The Autoignition of Hydrocarbon Fueled at High Temperatures and Pressures–Fitting of a Mathematical Model," Combustion Flame, Vol. 30, pp. 45-60, 1977

[9]. Kong, S. -C., Han Z., and Reitz, R. D., "The Development and Application of a Diesel Ignition and Combustion Model for Multidimensional Engine Simulation," SAE paper 950278, 1995

[10]. Magnussen, B.F. and Hjertager, B.H. "On mathematical modeling of turbulent combustion with special emphasis on soot formation and combustion." Sixteenth International Symposium on Combustion. Pittsburgh: The Combustion Institute, 1977.

[11]. Heywood, J. B., Internal Combustion Engine Fundamentals, McGraw-Hill, New York, NY, 1988.

[12]. Hiroyasu, H. and Kadota, T.," Models for Combustion and Formation of Nitric Oxide and Soot in DI Diesel Engines," SAE paper 760129, 1976.

[13]. Hiroyasu, H., Nishida, K., "Simplified Three-Dimensional Modeling of Mixture Formation and Combustion in a D.I. Diesel Engine," SAE Paper NO.890269, 1989

[14]. Nagle, J., Strickland-Constable, R. F., "Oxidation of Carbon between 1000-2000 C," Proc. Of the Fifth Carbon Conf., 1, 154, 1962